

# Chalcogen Atom-Doped Graphene and Its Performance in N<sub>2</sub> Activation

Navaratnarajah Kuganathan <sup>1,2</sup> 
<sup>1</sup> Department of Materials, Imperial College London, London SW7 2AZ, UK; n.kuganathan@imperial.ac.uk or ad0636@coventry.ac.uk

<sup>2</sup> Faculty of Engineering, Environment and Computing, Coventry University, Priory Street, Coventry CV1 5FB, UK

**Abstract:** In this work, we studied dispersion correction, adsorption and substitution of chalcogen dopants (O, S, Se and Te) on the surface of graphene using density functional theory. The results reveal that a single oxygen atom is more preferred for adsorption onto the graphene surface than the other dopants, with an adsorption energy of  $-0.84$  eV. The preference of this dopant is evidenced by a greater charge transfer of 0.34 electrons from the graphene surface to the oxygen. The substitutional doping of oxygen is energetically more favourable than the doping of other atoms. While nitrogen activation is enhanced by the adsorption, the activation is not significant with the doping of chalcogen atoms.

**Keywords:** graphene; density functional theory; molecular dinitrogen; adsorption



**Citation:** Kuganathan, N. Chalcogen Atom-Doped Graphene and Its Performance in N<sub>2</sub> Activation. *Surfaces* **2022**, *5*, 228–237. <https://doi.org/10.3390/surfaces5020016>

Academic Editor: Gaetano Granozzi

Received: 28 December 2021

Accepted: 8 March 2022

Published: 1 April 2022

**Publisher's Note:** MDPI stays neutral with regard to jurisdictional claims in published maps and institutional affiliations.



**Copyright:** © 2022 by the author. Licensee MDPI, Basel, Switzerland. This article is an open access article distributed under the terms and conditions of the Creative Commons Attribution (CC BY) license (<https://creativecommons.org/licenses/by/4.0/>).

## 1. Introduction

Graphene is one of the allotropes of carbon, consisting of a two-dimensional mono layer of carbon atoms with sp<sup>2</sup> hybridization [1–4]. Due to its remarkable mechanical, thermal, chemical and electrical properties, graphene is considered to be a versatile material with many applications in areas such as electronics, optics and energy storage systems [5–13].

The doping of graphene with hetero atoms (n-type or p-type impurities) has been shown to be an efficient way of altering its electrochemical performance and electronic properties [14–17]. The doping of B led to a significant charge transfer, and a negatively charged graphene surface was identified as a host material for adsorbing pollutants such as heavy metals [18–21]. Si-doped graphene has many potential applications, including serving as a catalyst for the reduction of CO<sub>2</sub> [22–24]. Using N-doped graphene, significant improvement has been achieved in the properties of fuel cells, Li-ion batteries and super capacitors [25–27].

Non-metal dopants such as S, P, F and I are reported to be promising catalysts for oxygen reduction reactions [28–32]. While there are many experimental studies available in the literature on doped graphene, a significant amount of theoretical work based on density functional theory (DFT) has also been reported [33–36].

In this study, we use spin-polarized DFT together with dispersion correction to examine the structures of chalcogen atoms (O, S, Se and Te) adsorbed and substitutionally doped graphene surfaces. Furthermore, activation of nitrogen molecules on the surfaces of adsorbed and doped graphene is studied.

## 2. Computational Methods

All calculations were performed using a plane wave DFT simulation code VASP (Vienna ab initio simulation program) [37]. Kohn–Sham (KS) equations are solved using plane wave basis sets and projected augmented wave (PAW) potentials [38]. A plane wave basis set with a cut-off of 500 eV was used in all calculations. The generalized gradient approximation (GGA) as formulated by Perdew, Burke and Ernzerhof (PBE) [39] was used to describe the exchange-correlation term. All structures were relaxed with the aid of

a conjugate gradient algorithm [40]. In all relaxed configurations, forces on the atoms were smaller than 0.001 eV/Å. A supercell with dimensions of  $25.5 \text{ Å} \times 14.75 \text{ Å} \times 30 \text{ Å}$  was used to ensure that adjacent dopants or molecules do not interact each other. A  $4 \times 4 \times 1$  Monk-horst [41] k-point mesh was used to optimize all configurations. Bulk diamond and graphite were optimized using  $8 \times 8 \times 8$  and  $8 \times 8 \times 4$  k point meshes, respectively. A semi-empirical method describing dispersive interactions was used as modelled by Grimme et al. [42]. Bader charge analysis [43] was used to calculate the charges on the dopants and C atoms on the graphene. Adsorption energy of a molecular nitrogen interacting with the atoms adsorbed or doped graphene surface was calculated using the following equation:

$$E_{\text{ads}} = E_{\text{N}_2@\text{M.Graphene}} - E_{\text{M.Graphene}} - E_{\text{N}_2} \quad (1)$$

where  $E_{\text{N}_2@\text{M.Graphene}}$  is the total energy of a molecular nitrogen adsorbed or doped on the surface of metal doped on the graphene surface,  $E_{\text{M.Graphene}}$  is the total energy of a metal-doped graphene surface and  $E_{\text{N}_2}$  is the total energy of molecular nitrogen.

### 3. Results

#### 3.1. Validation of Simulation Parameters

First, we performed full geometry optimization calculations on diamond, graphite, bulk S<sub>8</sub>, bulk Se and bulk Te to obtain equilibrium lattice constants and compare them with corresponding experimental values [44–48] (see Table 1). There is good agreement between experimental and calculated values, showing the efficacy of the PAW potentials used in this study. In Figure 1, the density of states (DOS) is shown. Graphene is a semiconductor as reported in previous studies [49], in agreement with the present simulation.

#### 3.2. Adsorption of N<sub>2</sub> on the Graphene

A single nitrogen molecule was allowed to adsorb on the surface of pristine graphene. Three different configurations were considered (see Figure 2). In all cases, adsorption is endoergic with respect to the N<sub>2</sub> molecule, indicating that the molecule is more stable in the gas phase than on the graphene surface. This is evidenced by the longer C-N bond distances (3.00–3.10 Å). Furthermore, Bader charges on the N<sub>2</sub> molecules show that there is no charge transfer between N<sub>2</sub> molecule and graphene. However, both the N<sub>2</sub> molecule and graphene surface are slightly polarized. Exoergic adsorption energies are calculated in all cases with respect to the gas phase N atom. This is due to the exothermic formation energy of the N<sub>2</sub> molecule from gas phase N atoms.

#### 3.3. Adsorption of N<sub>2</sub> on the Graphene Adsorbed with O, S, Se and Te

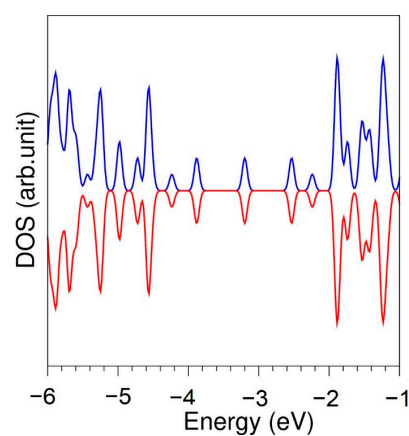
Next, chalcogen dopants were allowed to interact with pristine graphene. Three different initial configurations (66, C and H) were considered (see Figure 3). In configuration 66, the dopant atom is on the top of the C-C bond. The atom is on the top of a carbon in configuration C. In configuration H, the top of a hexagonal ring is occupied by a dopant atom. All initial configurations were allowed to relax. The relative energies of all dopants with respect to their most stable configuration (66) are shown in Table 2.

The results show that the most favourable position for all dopants is the 66 position (see Table 2). Other configurations exhibit slightly higher energy.

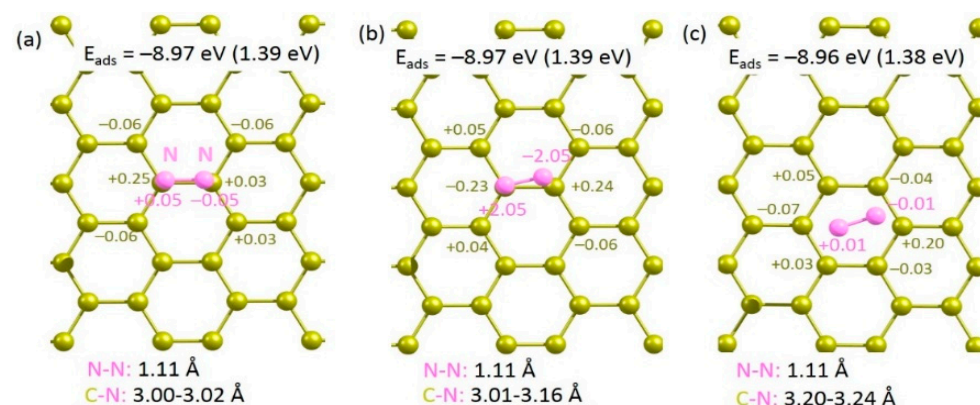
Relaxed structures showing the chalcogen atoms adsorbing on the 66 position of graphene is given in Figure 4a–d. Charge density plots associated with the interaction of dopant atoms with graphene are shown in Figure 4e–f.

Table 3 reports the adsorption energies, Bader charges on the dopants and C-X bond distances in the most stable (66) configurations. In all cases, adsorption is exothermic, meaning that adsorbed configurations are stable. The strongest adsorption is due to the highest electron negativity of O (3.44) compared to other dopants [50]. This is further confirmed by the most negative Bader charge on O and the shortest C-O bond distance.

Adsorption decreases with decreasing electronegativity, decreasing Bader charge and increasing C-X bond distance (see Figure 4).



**Figure 1.** Density of states of graphene.



**Figure 2.** Relaxed structures of  $N_2$  (a–c) adsorbed onto the surface of pristine graphene.

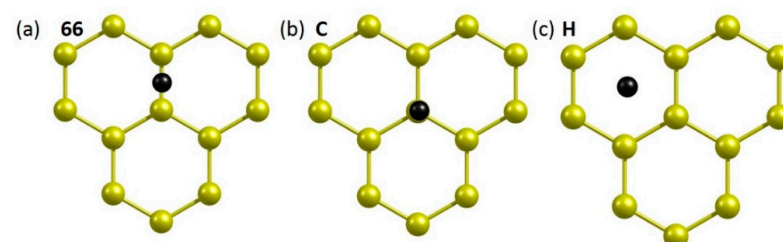


**Figure 3.** Initial configurations (a–c) of a dopant atom adsorbed onto the surface of pristine graphene.

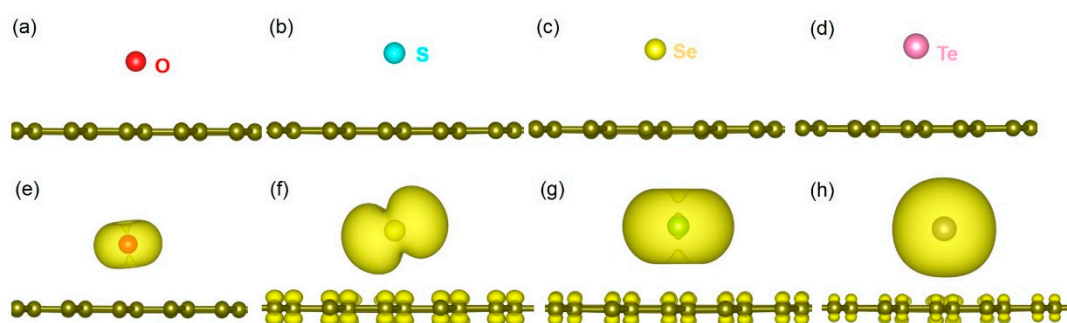


**Figure 4.** Relaxed structures of (a) O, (b) S, (c) Se and (d) Te adsorbed onto the graphene. Corresponding charge density plots associated with the adsorbed configurations (e–h) are also shown.

**Table 1.** Calculated and experimental lattice parameters of diamond, graphite, bulk S<sub>8</sub>, bulk Se and bulk Te.

Diamond [FM3M] [44]			
	Expt	Calc	Δ  (%)
a = b = c (Å)	3.567	3.573	0.31
α = β = γ (°)	90.0	90.0	0.00
Graphite [P6 <sub>3</sub> mc] [45]			
a = b (Å)	2.468	2.469	0.04
c (Å)	8.685	8.686	0.01
α = β (°)	90.0	90.0	0.00
γ (°)	120.0	120.0	0.00
Bulk S <sub>8</sub> [F d d d] [46]			
a (Å)	10.437	10.624	1.79
b (Å)	12.845	13.068	1.74
c (Å)	24.369	24.799	1.76
α = β = γ (°)	90.0	90.0	0.00
Bulk Se [P 31 2 1] [47]			
a = b (Å)	4.052	4.122	1.73
c (Å)	5.038	5.172	2.67
α = β (°)	90.0	90.0	0.00
γ (°)	120.0	120.0	0.00
Bulk Te [P 31 2 1] [48]			
a = b (Å)	4.456	4.413	0.96
c (Å)	5.921	5.942	0.35
α = β (°)	90.0	90.0	0.00
γ (°)	120.0	120.0	0.00

**Table 2.** Relative energies of three different configurations (66, C and H) of each dopant.

Atoms	Relative Energy (eV)		
	66	C	H
O	0.00	+0.01	+0.02
S	0.00	+0.03	+0.05
Se	0.00	+0.01	+0.02
Te	0.00	+0.01	+0.02

**Table 3.** Calculated adsorption energies, Bader charges on the dopant atoms and C-X bond distances in the most stable configuration—66.

Atom (X)	Electronegativity of X [50]	Adsorption Energy (eV)	Bader Charge on X ( e )	C-X (Å)
O	3.44	−0.84	−0.34	2.84
S	2.58	−0.55	−0.29	3.14
Se	2.55	−0.42	−0.26	3.25
Te	2.10	−0.35	−0.19	3.49

All doped configurations are still semiconductors (see Figure 5). However, p-states of dopant atoms are dispersed in the gap and the top of the valence band.

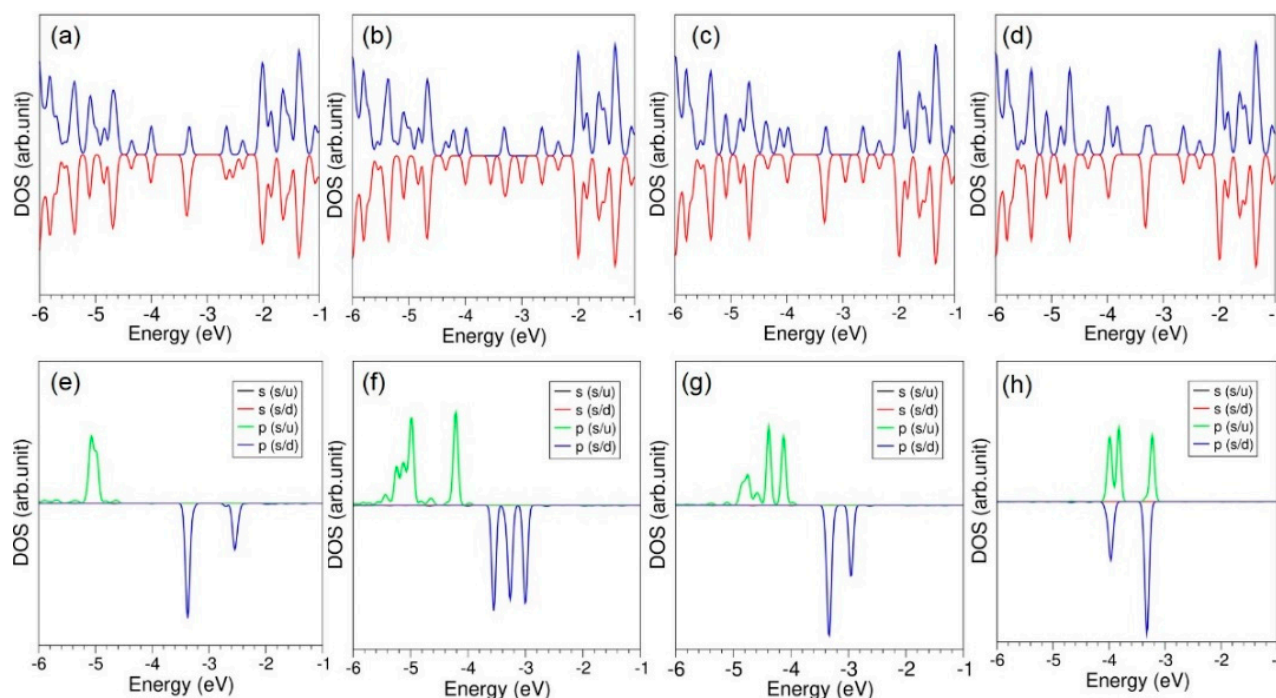


**Figure 5.** Total DOS plots of (a) O, (b) S, (c) Se and (d) Te adsorbed onto the graphene. Corresponding atomic DOS plots (e–h) are also shown.

Interaction of the  $N_2$  molecule on the surface of atoms adsorbed onto graphene is next considered next. Relaxed structures are shown in Figure 6. Table 4 reports the adsorption energies, Bader charges on  $N_2$  and adsorbed atoms, and the shortest bond distances. Calculations show that adsorption energies are positive, meaning that adsorption is unfavourable. Lower positive adsorption energies are calculated for O and S. This is reflected in the shorter O–N and S–N bond distances. In the case of Se and Te, Se–N and Te–N bond distances are longer than the O–N and S–N bond distances. This is reflected in the larger positive adsorption energies.

In the case of O and S, N–N bond distances are elongated significantly compared to that calculated for the gas phase  $N_2$  molecule (1.10 Å). Activation of  $N \equiv N$  is very small for Se and Te.

**Table 4.** Calculated adsorption energies, Bader charges on the  $N_2$  molecule and adsorbed atoms (X), and bond distances (C–X and N–N).

Configuration	Adsorption Energy (eV)	Bader Charge (e)		C–X (Å)	N–N (Å)
		X (X=O, S, Se and Te)	$N_2$		
O	+0.65	−0.31	+0.04, +0.13	2.76	1.195
S	+0.44	+0.14	−0.04, −0.14	2.87	1.182
Se	+1.26	−0.04	−0.01, −0.02	2.17	1.115
Te	+1.68	+0.08	+0.18, −0.26	2.42	1.119



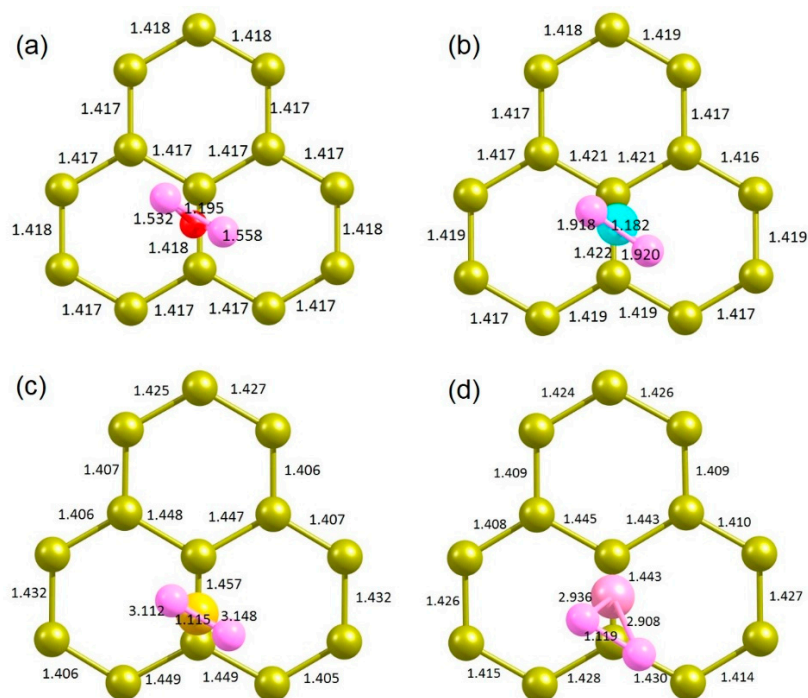


**Figure 6.** Relaxed structures of  $N_2$  interacting with (a) O, (b) S, (c) Se and (d) Te adsorbed onto the graphene.

### 3.4. Doping of O, S, Se and Te

Next, we considered the substitutional doping of chalcogen dopant atoms to enhance the degree of adsorption. Figure 7 shows the relaxed structures. The doped O forms a trigonal planar structure. The calculated substitution energy of O is 7.43 eV (Table 5). This indicates that the C–O bond is weaker than the C–C bond, as evidenced by the longer C–O bond length. This is partly due to the higher electronegativity of O than that of C. In the defect-free graphene, the C–C bond length is 1.41 Å. The C–O bond length is 0.06 Å longer than the C–C bond length in the pristine graphene (Figure 7a). The Bader charge analysis shows that the O atom gains 1.25 electrons from adjacent carbon atoms, leading to its higher electronegativity (3.44) than that of C (2.55) [50]. The valance band is occupied by the  $p$  states of O (see Figure 8a,e). Conversely, all other atoms form a trigonal pyramid structure in their relaxed structures (see Figure 7b–d). Substitution energy and C–X bond distance increase with increasing electronegativity. Bader charge analysis shows that there is a charge transfer from doped atoms to the nearest neighbour C atoms. Both S and Se exhibit similar +3.77 Bader charge, showing significant charge transfer. DOS plots show that  $p$  states of S, Se and Te are mainly occupied in the band gap region. Charge density plots show the electron distribution around the doped atoms and the nearest neighbour C atoms as observed in the Bader charge analysis.

**Table 5.** Calculated substitution energies, Bader charges on the doped atoms, and bond distances (C–X).

X in X@Graphene (X = O, S, Se and Te)	Electronegativity of X [50]	Substitution Energy (eV)	C–X (Å)	Bader Charge on X (e)
O	3.44	7.43	1.46	−1.25
S	2.58	8.33	1.74	+0.46
Se	2.55	9.77	1.89	+3.77
Te	2.10	11.06	2.06	+3.77

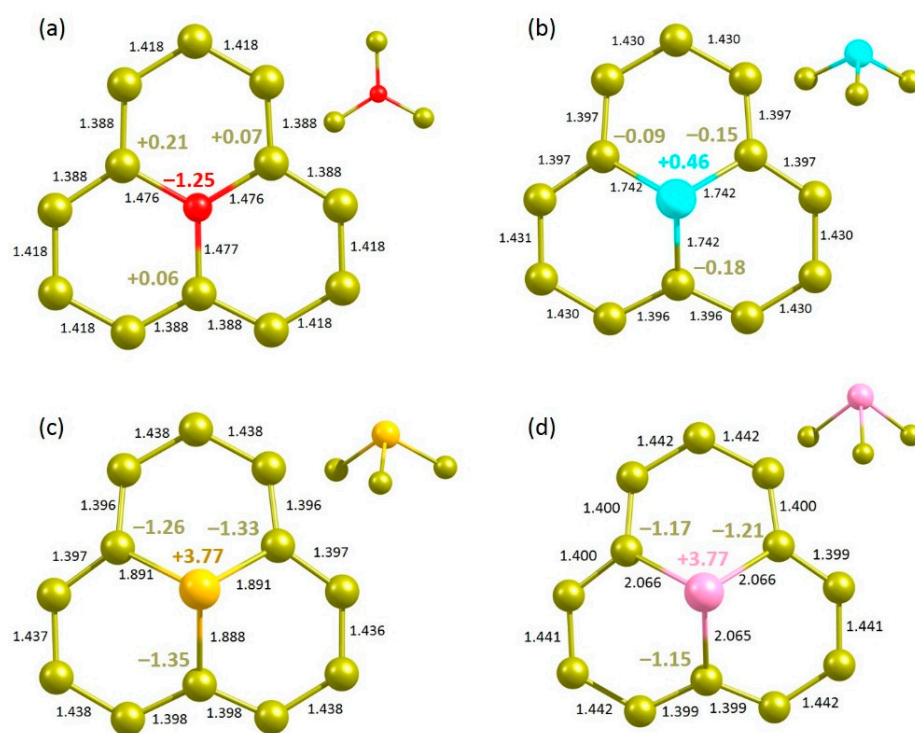


**Figure 7.** Relaxed structures of (a) O-, (b) S-, (c) Se- and (d) Te-doped graphene.

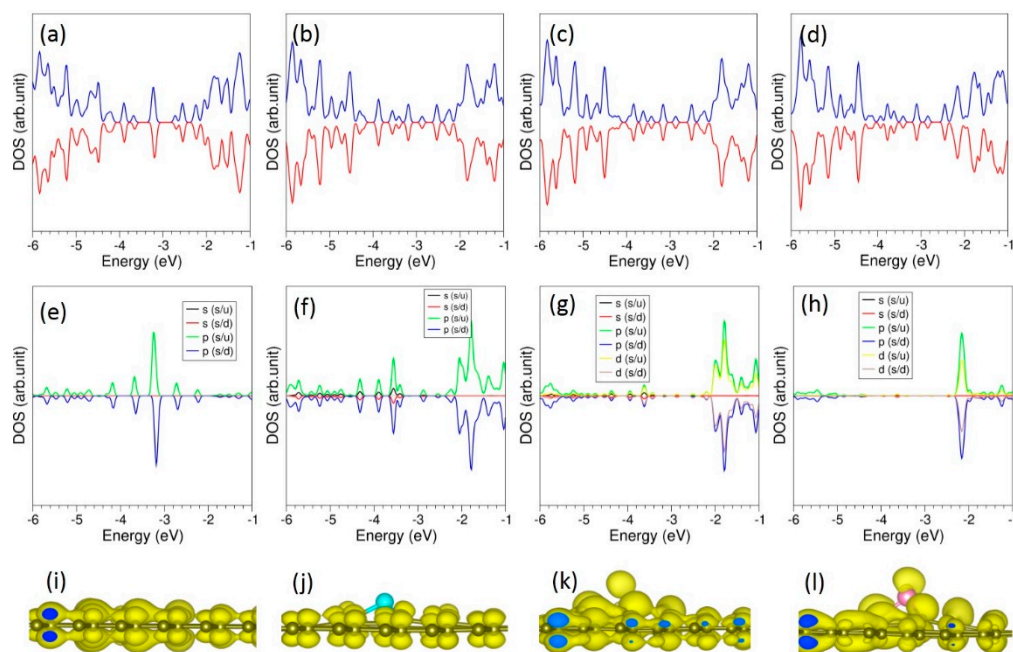


**Figure 8.** Total DOS plots of (a) O-, (b) S-, (c) Se- and (d) Te-doped graphene. Corresponding atomic DOS plots (e–h) and charge density plots associated with the doped atoms (i–l) are also shown.

DOS plots show that *p* states of S, Se and Te mainly occupy the band gap region (see Figure 8). Charge density plots show the electron distribution around the doped atoms and the nearest neighbour C atoms as observed in the Bader charge analysis.

### 3.5. $N_2$ Adsorption onto the Surface of Doped Graphene

Finally, the doped surface structures were considered for the adsorption of chalcogen atoms. The relaxed structures are shown in Figure 9. In the case of doping with O, exoergic

adsorption energy ( $-0.07$  eV) is calculated (see Table 6). Other dopants exhibit endoergic adsorption energies. Activation of the  $N_2$  molecule is very small, as evidenced by the very small elongation in the  $N \equiv N$  bond length. A very large positive adsorption energy of  $5.65$  eV is calculated for Te, meaning that this dopant is highly unfavourable.

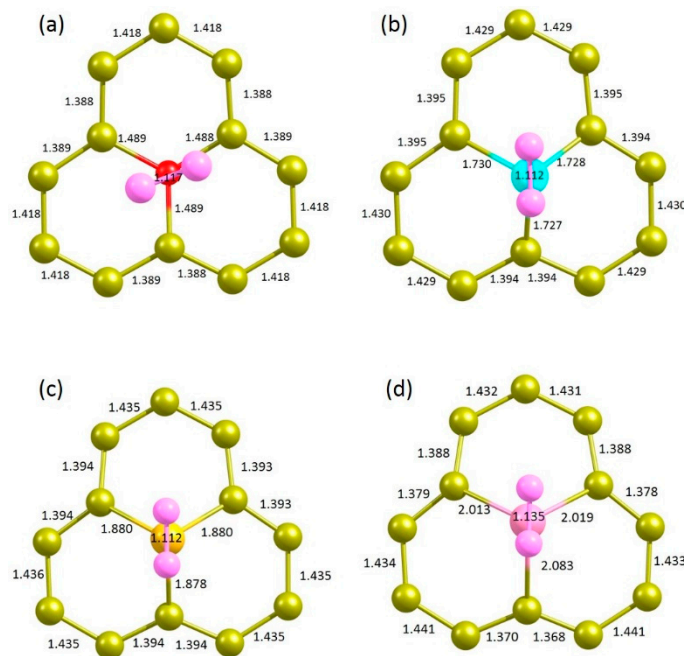


**Figure 9.** Relaxed structures of  $N_2$  adsorbed onto the (a) O-, (b) S-, (c) Se- and (d) Te-doped graphene.

**Table 6.** Calculated adsorption energies, Bader charges on the  $N_2$  molecule, and adsorbed atoms (X) and bond distances (C-X and N-N).

Configuration	Adsorption Energy (eV)	Bader Charge (e)		N-X (Å)	N-N (Å)
		X (X = O, S, Se and Te)	$N_2$		
O	$-0.07$	+0.18, +0.08, +0.08	$-2.04, +2.04$	3.03	1.12
S	+0.07	$-0.10, -0.17, -0.27$	$-0.10, +0.10$	3.16	1.11
Se	+0.27	$-0.37, -0.23, -0.28$	$-0.01, +0.01$	3.38	1.11
Te	+5.65	$-0.37, -0.23, -0.40$	$-0.16, -0.31$	3.47	1.14

#### 4. Conclusions

In this study, we report the structures and energetics of chalcogen atoms adsorbed and doped onto graphene using DFT simulations together with dispersion. We show that a single oxygen atom exhibits stronger adsorption than the other dopants. The adsorption energy is calculated to be  $-0.84$  eV. Such strong adsorption is evidenced by the charge transfer ( $0.34 e$ ) from the graphene surface to the oxygen. The most favourable atom for doping substitutionally on the surface is the oxygen. The adsorption enhances the nitrogen activation. Substitutional doping has no significant effect on nitrogen activation.

**Funding:** This research received no external funding.

**Data Availability Statement:** The data presented in this study are available upon reasonable request from the corresponding author.

**Acknowledgments:** High performance computing centre at Imperial College London is acknowledged for providing computational facilities.

**Conflicts of Interest:** The author declares no conflict of interest.



## References

1. Katsnelson, M.I. Graphene: Carbon in two dimensions. *Mater. Today* **2007**, *10*, 20–27. [\[CrossRef\]](#)
2. Allen, M.J.; Tung, V.C.; Kaner, R.B. Honeycomb Carbon: A Review of Graphene. *Chem. Rev.* **2010**, *110*, 132–145. [\[CrossRef\]](#)
3. Wu, Y.; Wang, S.; Komvopoulos, K. A review of graphene synthesis by indirect and direct deposition methods. *J. Mater. Res.* **2020**, *35*, 76–89. [\[CrossRef\]](#)
4. Tiwari, S.K.; Sahoo, S.; Wang, N.; Huczko, A. Graphene research and their outputs: Status and prospect. *J. Sci. Adv. Mater. Devices* **2020**, *5*, 10–29. [\[CrossRef\]](#)
5. Papageorgiou, D.G.; Kinloch, I.A.; Young, R.J. Mechanical properties of graphene and graphene-based nanocomposites. *Prog. Mater. Sci.* **2017**, *90*, 75–127. [\[CrossRef\]](#)
6. Sang, M.; Shin, J.; Kim, K.; Yu, K.J. Electronic and Thermal Properties of Graphene and Recent Advances in Graphene Based Electronics Applications. *Nanomaterials* **2019**, *9*, 374. [\[CrossRef\]](#) [\[PubMed\]](#)
7. Kim, Y.-J.; Kim, Y.; Novoselov, K.; Hong, B.H. Engineering electrical properties of graphene: Chemical approaches. *2D Mater.* **2015**, *2*, 042001. [\[CrossRef\]](#)
8. Lee, J.H.; Park, S.J.; Choi, J.W. Electrical Property of Graphene and Its Application to Electrochemical Biosensing. *Nanomaterials* **2019**, *9*, 297. [\[CrossRef\]](#)
9. Olabi, A.G.; Abdelkareem, M.A.; Wilberforce, T.; Sayed, E.T. Application of graphene in energy storage device—A review. *Renew. Sustain. Energy Rev.* **2021**, *135*, 110026. [\[CrossRef\]](#)
10. Syama, S.; Mohanan, P.V. Comprehensive Application of Graphene: Emphasis on Biomedical Concerns. *Nano-Micro Lett.* **2019**, *11*, 6. [\[CrossRef\]](#)
11. Madurani, K.A.; Suprpto, S.; Machrita, N.I.; Bahar, S.L.; Illiya, W.; Kurniawan, F. Progress in Graphene Synthesis and its Application: History, Challenge and the Future Outlook for Research and Industry. *ECS J. Solid State Sci. Technol.* **2020**, *9*, 093013. [\[CrossRef\]](#)
12. Dhinakaran, V.; Lavanya, M.; Vigneswari, K.; Ravichandran, M.; Vijayakumar, M.D. Review on exploration of graphene in diverse applications and its future horizon. *Mater. Today Proc.* **2020**, *27*, 824–828. [\[CrossRef\]](#)
13. Zheng, W.; Zhao, X.; Fu, W. Review of Vertical Graphene and its Applications. *ACS Appl. Mater. Interfaces* **2021**, *13*, 9561–9579. [\[CrossRef\]](#)
14. Chae, S.; Panomsuwan, G.; Bratescu, M.A.; Teshima, K.; Saito, N. p-Type Doping of Graphene with Cationic Nitrogen. *ACS Appl. Nano Mater.* **2019**, *2*, 1350–1355. [\[CrossRef\]](#)
15. Liu, H.; Liu, Y.; Zhu, D. Chemical doping of graphene. *J. Mater. Chem.* **2011**, *21*, 3335–3345. [\[CrossRef\]](#)
16. Meng, X.; Tongay, S.; Kang, J.; Chen, Z.; Wu, F.; Li, S.-S.; Xia, J.B.; Li, J.; Wu, J. Stable p- and n-type doping of few-layer graphene/graphite. *Carbon* **2013**, *57*, 507–514. [\[CrossRef\]](#)
17. Du, J.; Duan, J.; Yang, X.; Duan, Y.; Zhou, Q.; Tang, Q. p-Type Charge Transfer Doping of Graphene Oxide with (NiCo)<sub>1-y</sub>FeyOx for Air-Stable, All-Inorganic CsPbBr<sub>2</sub> Perovskite Solar Cells. *Angew. Chem. Int. Ed.* **2021**, *60*, 10608–10613. [\[CrossRef\]](#) [\[PubMed\]](#)
18. Feng, L.; Qin, Z.; Huang, Y.; Peng, K.; Wang, F.; Yan, Y.; Chen, Y. Boron-, sulfur-, and phosphorus-doped graphene for environmental applications. *Sci. Total Environ.* **2020**, *698*, 134239. [\[CrossRef\]](#)
19. Han, J.; Zhang, L.L.; Lee, S.; Oh, J.; Lee, K.S.; Potts, J.R.; Ji, J.; Zhao, X.; Ruoff, R.S.; Park, S. Generation of B-Doped Graphene Nanoplatelets Using a Solution Process and Their Supercapacitor Applications. *ACS Nano* **2013**, *7*, 19–26. [\[CrossRef\]](#) [\[PubMed\]](#)
20. Sahoo, M.; Sreena, K.P.; Vinayan, B.P.; Ramaprabhu, S. Green synthesis of boron doped graphene and its application as high performance anode material in Li ion battery. *Mater. Res. Bull.* **2015**, *61*, 383–390. [\[CrossRef\]](#)
21. Wang, H.; Zhou, Y.; Wu, D.; Liao, L.; Zhao, S.; Peng, H.; Liu, Z. Synthesis of Boron-Doped Graphene Monolayers Using the Sole Solid Feedstock by Chemical Vapor Deposition. *Small* **2013**, *9*, 1316–1320. [\[CrossRef\]](#) [\[PubMed\]](#)
22. Fang, L.; Cao, Z. CO<sub>2</sub> activation at atomically dispersed Si sites of N-doped graphenes: Insight into distinct electron mechanisms from first-principles calculations. *AIP Adv.* **2021**, *11*, 115302. [\[CrossRef\]](#)
23. Kuganathan, N.; Anurakavan, S.; Abiman, P.; Iyngaran, P.; Gkanas, E.I.; Chroneos, A. Adsorption of lead on the surfaces of pristine and B, Si and N-doped graphene. *Phys. B Condens. Matter* **2021**, *600*, 412639. [\[CrossRef\]](#)
24. Chen, Y.; Liu, Y.J.; Wang, H.X.; Zhao, J.X.; Cai, Q.H.; Wang, X.Z.; Ding, Y.H. Silicon-Doped Graphene: An Effective and Metal-Free Catalyst for NO Reduction to N<sub>2</sub>O? *ACS Appl. Mater. Interfaces* **2013**, *5*, 5994–6000. [\[CrossRef\]](#)
25. Su, H.; Hu, Y.H. Recent advances in graphene-based materials for fuel cell applications. *Energy Sci. Engin.* **2021**, *9*, 958–983. [\[CrossRef\]](#)
26. Yoo, E.; Nakamura, J.; Zhou, H. N-Doped graphene nanosheets for Li–air fuel cells under acidic conditions. *Energy Environ. Sci.* **2012**, *5*, 6928–6932. [\[CrossRef\]](#)
27. Ellessawy, N.A.; El Nady, J.; Wazeer, W.; Kashyout, A.B. Development of High-Performance Supercapacitor based on a Novel Controllable Green Synthesis for 3D Nitrogen Doped Graphene. *Sci. Rep.* **2019**, *9*, 1129. [\[CrossRef\]](#)
28. Yang, Z.; Yao, Z.; Li, G.; Fang, G.; Nie, H.; Liu, Z.; Zhou, X.; Chen, X.; Huang, S. Sulfur-Doped Graphene as an Efficient Metal-free Cathode Catalyst for Oxygen Reduction. *ACS Nano* **2012**, *6*, 205–211. [\[CrossRef\]](#)
29. Shen, B.; Chen, J.; Yan, X.; Xue, Q. Synthesis of fluorine-doped multi-layered graphene sheets by arc-discharge. *RSC Adv.* **2012**, *2*, 6761–6764. [\[CrossRef\]](#)

30. Yao, Z.; Nie, H.; Yang, Z.; Zhou, X.; Liu, Z.; Huang, S. Catalyst-free synthesis of iodine-doped graphene via a facile thermal annealing process and its use for electrocatalytic oxygen reduction in an alkaline medium. *Chem. Commun.* **2012**, *48*, 1027–1029. [[CrossRef](#)]
31. Li, R.; Wei, Z.; Gou, X.; Xu, W. Phosphorus-doped graphene nanosheets as efficient metal-free oxygen reduction electrocatalysts. *RSC Adv.* **2013**, *3*, 9978–9984. [[CrossRef](#)]
32. Albero, J.; Vidal, A.; Migani, A.; Concepción, P.; Blancafort, L.; García, H. Phosphorus-Doped Graphene as a Metal-Free Material for Thermochemical Water Reforming at Unusually Mild Conditions. *ACS Sustain. Chem. Eng.* **2019**, *7*, 838–846. [[CrossRef](#)]
33. Liu, A.; Guan, W.; Wu, K.; Ren, X.; Gao, L.; Ma, T. Density functional theory study of nitrogen-doped graphene as a high-performance electrocatalyst for CO<sub>2</sub>RR. *Appl. Surf. Sci.* **2021**, *540*, 148319. [[CrossRef](#)]
34. Tyagi, J.; Sharma, L.; Kakkar, R. Graphene and doped graphene: A comparative DFT study. *Adv. Mater. Lett.* **2019**, *10*, 484–490. [[CrossRef](#)]
35. Fang, Z.; Wang, Q.; Li, Y.; Li, Y.; Huang, S.; Lin, W.; Chen, W.; Zhang, Y. Theoretical insights into the thermal reduction of N<sub>2</sub> to NH<sub>3</sub> over a single metal atom incorporated nitrogen-doped graphene. *J. Chem. Phys.* **2021**, *154*, 054703. [[CrossRef](#)]
36. Askari Ardehjani, N.; Farmanzadeh, D. DFT investigation of metal doped graphene capacity for adsorbing of ozone, nitrogen dioxide and sulfur dioxide molecules. *Adsorption* **2019**, *25*, 661–667. [[CrossRef](#)]
37. Kresse, G.; Furthmüller, J. Efficient iterative schemes for ab initio total-energy calculations using a plane-wave basis set. *Phys. Rev. B* **1996**, *54*, 11169–11186. [[CrossRef](#)]
38. Blöchl, P.E. Projector augmented-wave method. *Phys. Rev. B* **1994**, *50*, 17953–17979. [[CrossRef](#)]
39. Perdew, J.P.; Burke, K.; Ernzerhof, M. Generalized Gradient Approximation Made Simple. *Phys. Rev. Lett.* **1996**, *77*, 3865–3868. [[CrossRef](#)]
40. Press, W.H.; Teukolsky, S.A.; Vetterling, W.T.; Flannery, B.P. *Numerical Recipes in C: The Art of Scientific Computing*, 2nd ed.; Cambridge University Press: New York, NY, USA, 1992.
41. Monkhorst, H.J.; Pack, J.D. Special points for Brillouin-zone integrations. *Phys. Rev. B* **1976**, *13*, 5188–5192. [[CrossRef](#)]
42. Grimme, S.; Antony, J.; Ehrlich, S.; Krieg, H. A consistent and accurate ab initio parametrization of density functional dispersion correction (DFT-D) for the 94 elements H–Pu. *J. Chem. Phys.* **2010**, *132*, 154104. [[CrossRef](#)] [[PubMed](#)]
43. Bader, R.F.W. The zero-flux surface and the topological and quantum definitions of an atom in a molecule. *Theor. Chem. Acc.* **2001**, *105*, 276–283. [[CrossRef](#)]
44. Yamanaka, T.; Morimoto, S. Isotope effect on anharmonic thermal atomic vibration and [kappa] refinement of 12C and 3C diamond. *Acta Crystallogr. Sect. B* **1996**, *52*, 232–238. [[CrossRef](#)]
45. Bosak, A.; Krisch, M.; Mohr, M.; Maultzsch, J.; Thomsen, C. Elasticity of single-crystalline graphite: Inelastic x-ray scattering study. *Phys. Rev. B* **2007**, *75*, 153408. [[CrossRef](#)]
46. Abrahams, S. The crystal and molecular structure of orthorhombic sulfur. *Acta Crystallogr.* **1955**, *8*, 661–671. [[CrossRef](#)]
47. Keller, R.; Holzapfel, W.B.; Schulz, H. Effect of pressure on the atom positions in Se and Te. *Phys. Rev. B* **1977**, *16*, 4404–4412. [[CrossRef](#)]
48. Adenis, C.; Langer, V.; Lindqvist, O. Reinvestigation of the structure of tellurium. *Acta Crystallogr. Sect. C* **1989**, *45*, 941–942. [[CrossRef](#)]
49. Singh, S.; Faraz, M.; Khare, N. Recent Advances in Semiconductor–Graphene and Semiconductor–Ferroelectric/Ferromagnetic Nanoheterostructures for Efficient Hydrogen Generation and Environmental Remediation. *ACS Omega* **2020**, *5*, 11874–11882. [[CrossRef](#)]
50. Lide, D.R. *CRC Handbook of Chemistry and Physics*; ACS Publications: Florida, CA, USA, 2008; pp. 12–114.